Chapter 4

Robust and highly compressible polyacrylamide co-polymer hydrogel developed through g-C_3N_4 initiated photopolymerisation and its photocatalytic activity towards dye removal

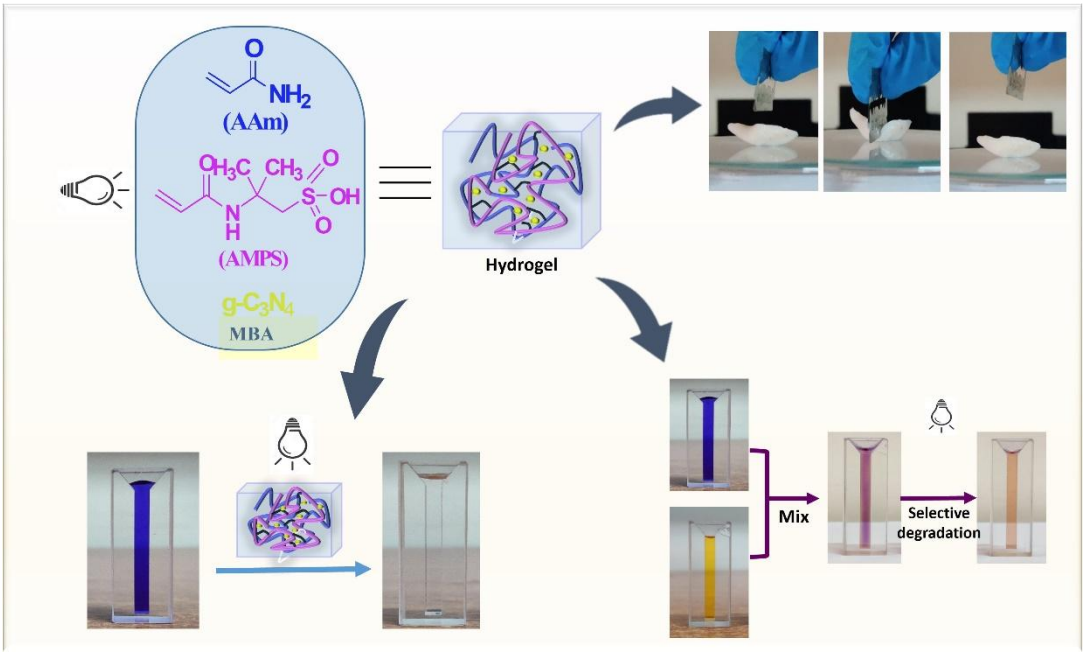

This chapter describes the fabrication of a photocatalytic hydrogel utilizing g-C_3N_4 as a photoinitiator. The research investigates the photocatalytic properties of the synthesized hydrogel by employing it to remove organic dyes and studying the combined effect of adsorption and photodegradation for dye removal.

Parts of this thesis work are published as:

Ahmed, A., Saikia, P., Ray, P., Dutta, R. and Dolui, S.K. A robust and highly compressible polyacrylamide co-polymer hydrogel developed through g-C_3N_4 initiated photopolymerisation and its photocatalytic activity towards dye removal. ***New Journal of Chemistry***, 48(9):3984-3997, 2024.

4.1 Introduction

Hydrogel, being a soft material, can be easily deformed and has attracted widespread attention to society. The high water holding capacity and tunable physical and chemical properties in hydrogel have made it highly advantageous over other soft materials and can be employed in a wide range of industrial applications such as wastewater treatment, agriculture, oil recovery, and the food industry [1-6]. For many years, wastewater treatment has become an important part of water management as industries and factories have been releasing dyes and other toxic substances to the water bodies at an alarming rate. Thus, efforts have been devoted to recycling water through the adsorption or degradation of pollutants. Among the various purification techniques, photocatalytic degradation has been widely used because of its easy application and high efficiency [7,8]. Although various nano photocatalytic materials exhibit high photodegradation efficiency, the difficulties in their separation from water bodies possess secondary pollution. Much research work has been dedicated to where nanomaterials are loaded into materials such as glass, metal, plastics, polymers, hydrogels, or ceramics to increase catalytic efficiency [9-11]. As already discussed in Chapter 1, hydrogels stood out to be highly advantageous over other immobilizing photocatalytic materials because of their high transmittance, easy and high catalyst loading capability, good biocompatibility, high specific surface areas, easy recovery, and recyclability. Moreover, the high swelling capacity of the hydrogel allows easy diffusion of the pollutant into the hydrogel matrix. Therefore, conjoining hydrogel with photoactive material results in a photoactive hydrogel with a wide range of economic anticipation, especially for wastewater remediation [12-15]. Although, hydrogel found numerous applications in wastewater treatment, its mechanical strength and recyclability which are the most crucial properties of an adsorbent are often neglected. In a work by Yang *et al*., a polymer (N-methyl maleic acid/hydroxyethyl acrylate) hydrogel for the adsorption and degradation of Sulphamethoxazole has been developed. Under 500W visible light, they can remove 95.91% of the pollutant [16]. Again, Sharma *et al*. in their work, demonstrate a combined photocatalytic degradation of a mixture of malachite green and fast green dye by starch-based nanocomposite hydrogel [17]. In a similar work, Al-Aidy *et al*. showed the removal of malachite green dyes using starch-based hydrogel adsorbents with an adsorption capacity of 18.36mg/g [18]. Shaifee *et al*. developed a g-C_3N_4/Co_3O_4/MWCNT composite hydrogel for the removal of Rhodamine B by a synergy

of adsorption and photocatalysis. They obtained a maximum removal of 87% within 120 min [19]. In another work, Zhao *et al*. developed titanium dioxide-embedded sodium alginate and acrylamide composite film for dye degradation with a tensile strength of 0.316 MPa. The film shows reusability for up to 5 cycles [20]. Again Gao *et al*. synthesized a TiO_2 embedded hyaluronic acid hydrogel for the photodegradation of dyes with a maximum tensile strength of 0.304 MPa [21]. Although the above-discussed hydrogels showed good dye removal performance, many works possess potential limitations as they have ignored the mechanical and recyclable properties. However, in some works, mechanical strength has been discussed but was found to be quite poor. Therefore, developing hydrogel with sufficient mechanical properties and good recyclability is crucial to withstand the desired application.

Traditionally, hydrogels are synthesized by a thermally induced free radical polymerization reaction. However, hydrogel synthesis *via* photo-polymerization has become an advancing technological approach in polymer science as it is less time-consuming, requires low input energy, is environmentally friendly, and has good control over spatial arrangement [22, 23]. Therefore, research has been carried out to develop an efficient photoinitiator with a suitable absorption spectrum under visible light. In that regard, graphitic carbon nitride (g-C_3N_4) has been introduced as a metal-free semiconductor photocatalyst that satisfies the basic requirement of an efficient photocatalyst. It comprises a layered sheet held together by weak Van der Waals forces [24]. Each sheet consists of a regular arrangement of tri-s-triazine units obtained by thermal condensation of low-cost and abundant precursors. These precursors are generally carbon and nitrogen-containing compounds such as melamine, urea, dicyandiamide, thiourea, and cyanimide [25]. With a tunable band gap of around 1.8-2.7 eV, g-C_3N_4 acts as an excellent metal-free semiconductor, capable of being excited by visible light. In recent years, g-C_3N_4 has been investigated as a radical initiator for polymerisation reactions. Kiskan et.al. used mesoporous graphitic carbon nitride as a radical initiator in visible-light induced polymerization and by using tertiary amine as a co-initiator [26]. In another work, Kumuru and his co-workers have utilized g-C_3N_4 as a photoinitiator for the formation of hydrogel with reinforced properties [27]. Owing to its unique physicochemical stability, non-toxicity, low price, facile synthesis, and good catalytic and light harvesting properties, it has attracted significant interest in its use as a photocatalyst in water splitting, CO_2 reduction, metal-ion reduction, sensing, and

imaging. In addition, its photodegradation property has found immense application in water remediation. Akhundi *et al*. demonstrate a successful preparation of g-C_3N_4/ZnO/AgCl nanocomposites for photodegradation of Rhodamine B. They found that the photocatalytic activity of synthesized nanocomposite is 9.5 times higher than g-C_3N_4 which may be due to the efficient separation of the charge carriers by the synergistic effect of ZnO and AgCl in removing photogenerated electrons from g-C_3N_4 [28]. Again, a work by Quan *et al*. has prepared g-C_3N_4/Bi@Bi_2WO_6 composite photocatalyst for hydrogen production and photocatalytic degradation of RhB and TC. They found that the rate of both hydrogen production and photodegradation was much higher than the pure g-C_3N_4. These enhanced photocatalytic effects were caused by the synergies of the 2D/2D coupling interface and the deposited metal Bi [29]. In a similar work by Tian *et al*. developed a ternary g-C_3N_4/MoS_2/graphene nanocomposite photocatalyst which again shows photodegradation of RhB with a rate which is 4.8 times higher than that of pure g-C_3N_4 under visible light irradiation [30] Similarly Bao and his co-workers synthesized a $LaNiO_3$/g-C_3N_4/MoS_2 Z-scheme heterogeneous nanostructure as a photocatalyst for water splitting, photodegradation of TC, and Cr(VI) reduction and it was found to exhibit enhanced photocatalytic performance [31]. Therefore, g-C_3N_4 has been incorporated into the hydrogel matrix for developing photocatalytic hydrogels. Cao et.al developed a macrogel by utilizing g-C_3N_4 as a photoinitiator. They also demonstrate the photocatalytic properties of the gel [32]. Therefore, incorporating g-C_3N_4 into a 3D hydrogel matrix shows not only photocatalytic behavior but also improves the overall mechanical properties of the hydrogel by acting as a reinforcing agent [33-35]. Although, many works were found on g-C_3N_4 composite hydrogel. Nonetheless, only a few works have been done in synthesizing photocatalytic hydrogel by employing g-C_3N_4 as a photoinitiator.

In this chapter, we have developed a facile and one-step procedure to synthesize a photocatalytic hydrogel by the co-polymerization of 2-acrylamido-2-methylpropane sulphonic acid (AMPS) and acryl amide (AAm) by employing visible light irradiation and g-C_3N_4 as a photoinitiator. The co-polymerization of AMPS with AAm increases the swelling capability of the hydrogel which is attributed to the an ionizable sulphonic group [36]. The developed hydrogel shows good mechanical properties with extreme compressibility and possesses excellent photocatalytic activity towards the degradation of different organic dyes with high selectivity towards cationic dyes. It was found that

the readily swellable properties of the hydrogel allow easy and fast diffusion of the contaminant particles into the gel network thereby resulting in fast photocatalytic degradation. Therefore, the synergistic effect of adsorption and degradation in g-C_3N_4 based hydrogel results in an efficient photocatalytic material. This implies that the synthesized hydrogel provides a simple, green, and cost-effective method for treating wastewater containing harmful cationic dyes.

4.2 Experimental sections

4.2.1 Materials

Acrylamide (AAm), melamine was purchased from Fluka. 2-Acrylamido-2-methyl-1-propanesulphonic acid (AMPS) and *N,N´*-methylenebis(acrylamide) (MBA), crystal violet (CV), rhodamine B (RhB), methylene blue (MB) and methyl orange (MO) were purchased from Sigma Aldrich. Ammonium persulfate (APS) was obtained from Merck. Deionized water was used during the experiment for preparing various solutions. All the reagents used were of analytical grade and were used as received.

4.2.2 Synthetic procedures

4.2.2.1 Synthesis of bulk graphitic carbon nitride (g-C_3N_4)

Bulk g-C_3N_4 was synthesized by a thermal polymerization reaction reported previously [37]. Initially, 3 g of melamine powder was taken in a crucible and heated in a muffle furnace at 490 °C for about 5 hrs. The product thus obtained was ground to powder to get the bulk g-C_3N_4.

4.2.2.2 Synthesis of blank hydrogel (CN0)

0.8 g of AMPS and 0.4 g of AAm were taken in a glass vial with 5 mL of deionized water. 1 wt % MBA was then added to the prepared solution as a crosslinker. APS was dissolved in 1mL of water and added dropwise to the prepared solution. The mixture was then flushed with nitrogen for 15 min, and the reaction was kept on stirring for almost 4 hours. The obtained hydrogel was washed several times and dried for further use.

4.2.2.3 Synthesis of g-C_3N_4 based hydrogel (CN hydrogel)

In a 100 mL round-bottom flask, a calculated amount of g-C_3N_4 was dispersed in 4 mL of distilled water and allowed to undergo ultrasonication for 1 hour. After that 0.8 g of AMPS and 0.4 g of AAm, along with crosslinker MBA were added to the above dispersion. The reaction mixture was then flushed with a nitrogen atmosphere for 15

min. The solution was then placed in a light chamber containing two 50-watt white LED lights to initiate gelation. A white-colored gel was obtained within 1 hour. The resulting hydrogel was washed with distilled water to rinse out the unreacted particles. The detailed composition of the hydrogel was given in Table 4.1.

Table 4.1 Detailed composition of the CN hydrogels

Sl.no.	AAm (mg)	AMPS (mg)	g-C_3N_4 (wt% of total monomer content	Crosslinker (mg)	N_2	Light	Hydrogel
1	400	800	0.8	12	✓	✓	CN 0.8
2	400	800	1	12	✓	✓	CN1
3	400	800	2	12	✓	✓	CN2
4	400	800	3	12	✓	✓	CN3
5	400	800	4	12	✓	✓	CN4
6	400	800	5	12	✓	✓	CN5
7	400	800	0	12	✓	✓	No reaction
8	400	200	8	12	✓	✓	CN6
9	400	200	8	12	×	✓	No reaction
10	400	200	8	12	×	×	No reaction
11	400	200	8	12	✓	×	No reaction
12	400	200	8	0	✓	✓	Gel formed dissolves in water

4.3 Characterization

4.3.1 Structural characterization

The Fourier Transform Infrared (FTIR) spectral analysis, Scanning Electron Microscopy, Powder X-Ray Diffraction (XRD), And Thermal Stability of the hydrogel were recorded using the same instrumentation and similar methods as described in section 2.3 in Chapter 2.

4.3.2 Transmission Electron Microscopy (TEM)

TEM images were recorded using a Transmission Electron Microscope JEOL JEM 1400 instrument, Japan at 120 kV of acceleration voltage. The samples were prepared for TEM by dispersing them in ethanol solution.

4.3.3 UV-visible spectroscopy

A Shimadzu 2550 UV-visible spectrophotometer was used to record the UV-visible absorbance. Here, the samples were prepared by dispersing them in water.

4.3.4 CHN and Photoluminescence (PL) analysis

CHN analysis was done by using the Perkin Elmer CHN analyzer. Photoluminescence (PL) was performed by using Hitachi F-2700 fluorescence spectrophotometer. The compression tests on hydrogels were determined by using a Universal Testing Machine (UTM, Zwick, Z010).

4.3.5 Determination of equilibrium swelling of the hydrogel

For determining the swelling behavior of the hydrogel, a fixed amount of oven-dried hydrogel samples with different compositions of g-C_3N_4 were immersed in distilled water and different solutions of pH 1 and pH 10. The samples were then allowed to swell until an equilibrium swelling was reached. The swelling percentage of the hydrogel was calculated by using the formula:

$$\text{Swelling \%} = \frac{W_s - W_d}{W_d} \times 100\%$$

where W_s and W_d are the weights of the swollen and dehydrated samples respectively.

4.3.6 Photocatalytic activity study

The photocatalytic activity of the synthesized hydrogel was studied by the degradation of CV dye as a model organic pollutant in an aqueous solution. To study the effect of pH and g-C_3N_4 content on dye removal, batch experiments were carried out by immersing a fixed quantity (approx. 0.09 g) of different hydrogel samples into a 30 ml dye solution of 10 ppm concentration. The solution was then placed in the dark for 30 min to attain maximum swelling. After that, the solution containing the photocatalyst was placed in a light chamber containing two 50W white LED lights placed at 9 cm. Aliquots (1 ml) were then withdrawn at a specific time interval and the solution concentration was evaluated by using a UV-visible spectrophotometer. The UV-visible spectra of the samples were recorded between 200-800 nm.

The removal efficiency of the dye can be calculated by using the formula:

$$\text{Removal Efficiency \%} = \frac{C_0 - C_t}{C_0} \times 100\%$$

Where C_o is the concentration of the dye at time, t=0 min and C_t is the concentration of the dye at a specific time interval.

The kinetics of CV dye degradation were also explored using pseudo-first-order and pseudo-second-order kinetics models.

4.3.7 Selective behaviour to dyes

The selectivity of the hydrogel to different dyes was determined by performing experiments on different cationic dyes such as MB and RhB as well as anionic dye MO. Here, hydrogel samples were immersed in 30 ml of different dye solutions containing the above cationic and anionic dyes. The concentration of dye at different time intervals was measured using a UV-visible spectrophotometer. Moreover, the selectivity of the hydrogel was further confirmed by performing a similar experiment using a binary mixed dye solution containing CV and MO dye.

4.3.8 Recyclability study

To study the recyclability of the hydrogel, the dye-treated hydrogel was simply washed with distilled water and then oven-dried for de-swelling. The dried hydrogel thus obtained was again immersed in 30 ml dye solution and its dye removal efficiency was determined by using a UV-visible spectrophotometer. This cycle was repeated for 5 times to examine the recyclability of the synthesized hydrogel.

4.3.9 Adsorption property study

The adsorption property of the hydrogel towards the dye was also evaluated by immersing the hydrogel sample into a CV dye solution. The adsorption was investigated by taking out a volume of 1ml solution at a definite time interval until equilibrium and dye concentration were studied by using a UV-visible spectrophotometer. The whole experiment was performed under dark conditions and at room temperature.

The effect of adsorbent dosage and removal efficiency was evaluated by taking different adsorbent dosages ranging from 0.025 g to 0.1 g in a 30 ml dye solution with a concentration of 10 ppm. Similarly, the influence of initial dye concentration on dye adsorption was studied by varying the concentration of dye from 5 ppm to 50 ppm with an adsorbent dosage of 0.03g.

The adsorption capacity was calculated by using the equation:

$$Q = \frac{(C_0 - C_e)V}{m}$$

The adsorption percentage was calculated by using the equation:

$$R\% = \frac{C_0 - C_t}{C_0} \times 100\%$$

Where C_o is the concentration of the dye at time, t=0 min and C_t is the concentration of the dye at a specific time interval, C_e is the concentration of the dye at equilibrium, m(g) is the mass of the adsorbent; and V(L) is the volume of the adsorption solution.

The adsorption kinetics and adsorption mechanism of the hydrogel towards the dye solution were also determined.

4.4 Results and Discussion

4.4.1 Fabrication and characterization of photoactive hydrogel

The synthetic procedure for the fabrication of photoactive hydrogel follows a facile one-pot synthesis method. The g-C_3N_4 which acts as a photoinitiator for the polymerisation of hydrogel was first synthesized according to a previously reported pyrolysis method using melamine as a precursor. After dispersing g-C_3N_4 in water, the monomer AAm and AMPS along with crosslinker MBA were added to it and then degassed with N_2 atmosphere to remove dissolved oxygen. The photopolymerization reaction proceeds through a free radical polymerization reaction where g-C_3N_4 acts as a photoinitiator.

On light irradiation, the photo-generated electron, and holes on g-C_3N_4 surfaces initiate the formation of radicals on AMPS and AAm monomers. The polymer chain was further cross-linked by the end vinyl group of the crosslinking agent MBA and by g-C_3N_4 through the strong hydrogen bonding interactions to give three-dimensional crosslinked hydrogel. The formation of radicals on g-C_3N_4 surfaces was further determined by performing reactions by adding different radical scavengers and it was found that there was complete inhibition of gelation. The high photocatalytic activity of g-C_3N_4 provides a faster gelation rate resulting in the formation of hydrogel within 1 hr. In addition, as shown in Table 4.1, in group 7, g-C_3N_4 was not used during the reaction process, therefore on light irradiation, no radicals are generated hence, no hydrogel formation takes place. Similarly, no reaction occurred in group 9. This is due to the presence of O_2 atmosphere. Since molecular oxygen inhibits free radical polymerization reaction by scavenging the radical formed during the initiation of the reaction, resulting

in the formation of peroxy radical which retard the photopolymerization reaction. Therefore, reactions performed in the presence of oxygen gave a negligible product showing poor mechanical strength. The plausible mechanism of the hydrogel formation is shown in Scheme 4.1

Step 1: Synthesis of bulk graphitic carbon nitride (g-C_3N_4)

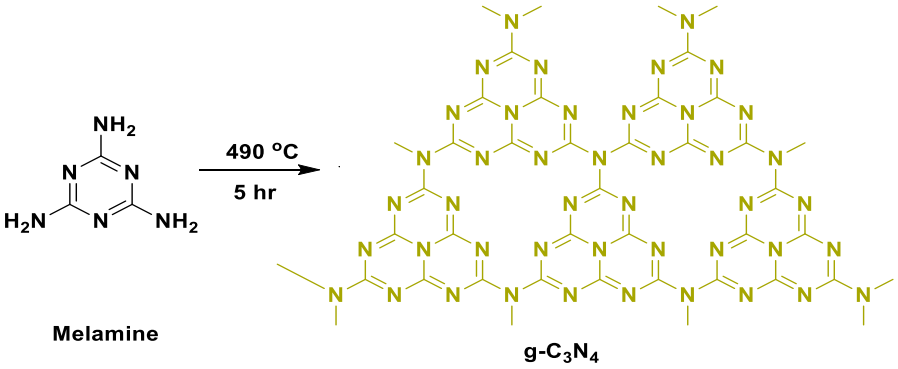

Step 2: Synthesis of g-C_3N_4 based hydrogel (CN hydrogel)

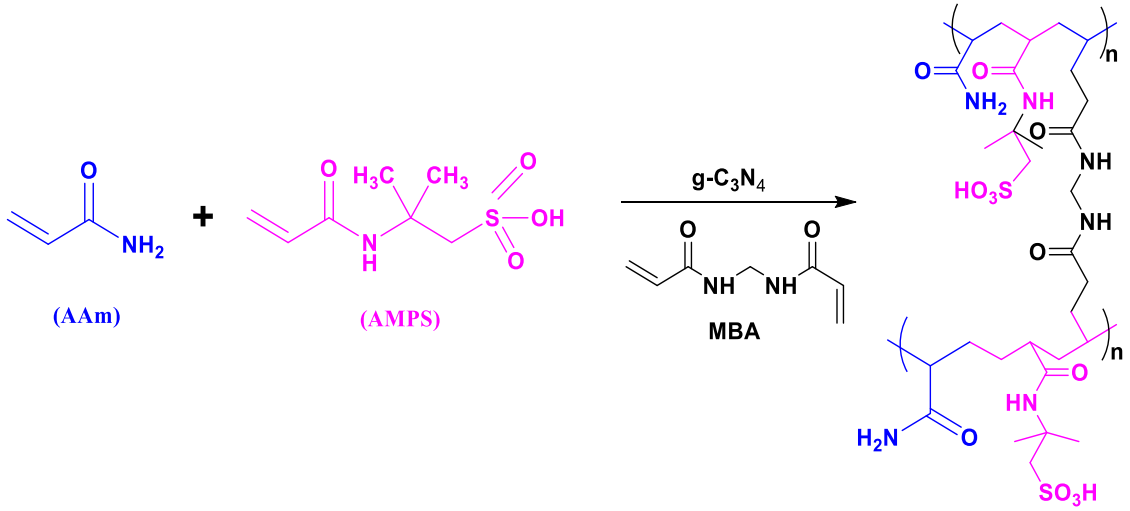

Scheme 4.1 Plausible mechanism of hydrogel formation

4.4.2 FTIR analysis

The formation of g-C_3N_4 can be determined from the FTIR spectral data as shown in Figure 4.1(a). The peak at 3080 cm^{-1} is due to the N-H group vibration present at the surface of carbon nitride or due to the stretching mode of the $–NH_2$ group, which are uncondensed amine groups. The strong bands at 1637 cm^{-1} and 1407 cm^{-1} were assigned to the aromatic CN stretching vibration. The intense peak at 803 cm^{-1} is attributed to the C-N heterocycles and is the characteristic peak of the triazine molecule.

Again, to determine the formation of hydrogel, FTIR spectroscopy has been carried out and the spectra are shown in Figure 4.1(b). The spectra of AAm and AMPS showed two peaks in the range of 1600-1700 cm-1 which can be assigned to C=C and C=O vibration. However, the spectra of hydrogel exhibit only a single peak in that region which is remarkable for C=O vibration. Again, in the range of 930-980 cm-1, two peaks were observed in the monomers which can be attributed to vinyl C-H bending but collapsed in the hydrogel. The appearance of a single peak at 1030 cm-1 might be due to the C-S-O group from AMPS [39]. Moreover, two sharp peaks at 2920 and 2850 cm^{-1} in the hydrogel can be attributed to methylene C-H symmetric and asymmetric vibration. Thus, occurrences of new peaks and shifts in the original peaks indicate the successful synthesis of the hydrogel. Moreover, as shown in Fig 4.1(c), the incorporation of g-C_3N_4 into the hydrogel matrix shows a shift in the N-H stretching from 3437 cm^{-1} to 3419 cm^{-1}. This shift towards lower wavenumber indicates the formation of H-bonding between the hydrogel matrix and g-C_3N_4. In addition, the appearance of a sharp peak at 809 cm^{-1} is due to the triazine unit of g-C_3N_4 [38].

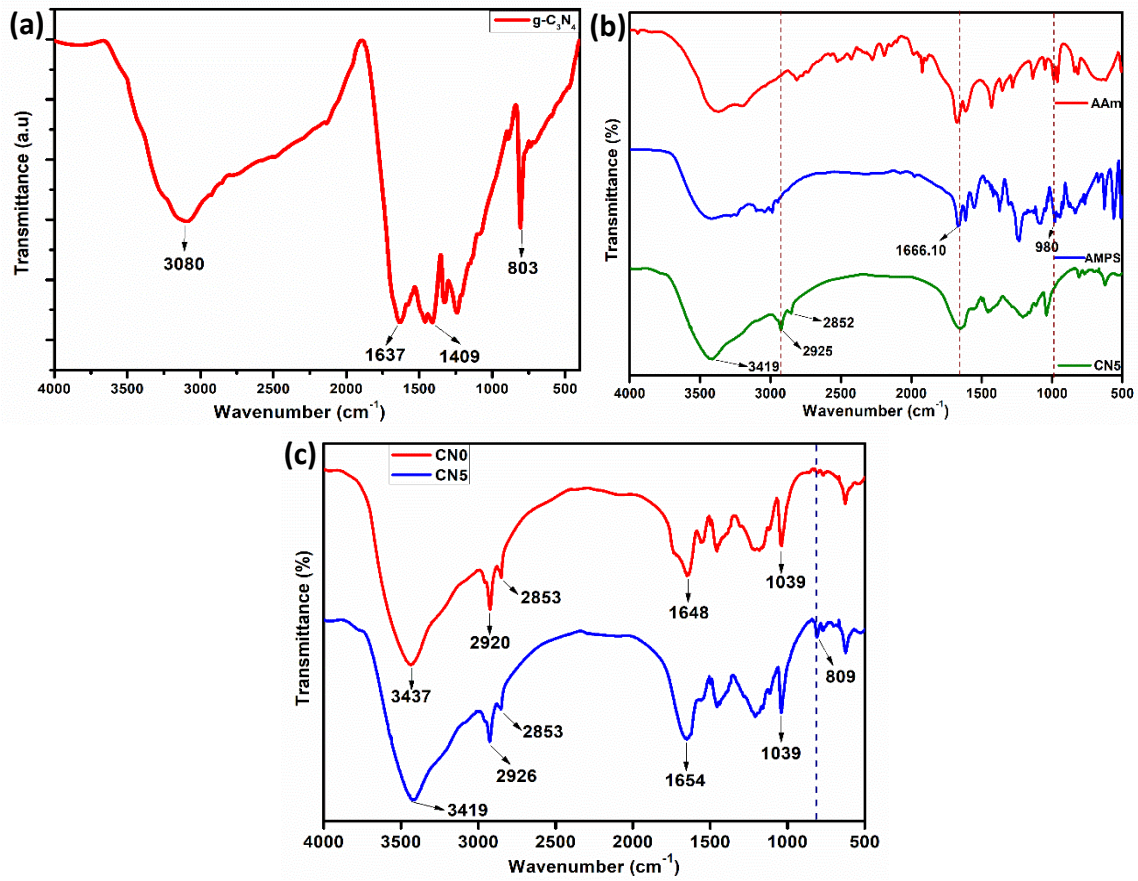

Figure 4.1 FTIR spectroscopy of (a) bulk g-C_3N_4, (b) AAm, AMPS monomers and CN5 hydrogel, (c) CN0 hydrogel and CN5 hydrogel

4.4.3 X-ray diffraction analysis (XRD)

The XRD pattern for g-C_3N_4 shows two peaks at around 13 ° and 27 ° as shown in Figure 4.2(a). The small characteristic peak at around 13 ° represents (1 0 0) facet which arises due to in-planar tri-s-triazine unit. The strongest characteristic peak at around 27 ° is indexed as (002) facet, which is usually seen in graphitic materials because of the interaction of the interlayer stacking in the conjugated aromatic system

Again, XRD analysis of the blank hydrogel (CN0, without g-C_3N_4) and g-C_3N_4 incorporated hydrogel (CN hydrogel) have been examined. From Figure 4.2(b), it is seen that the g-C_3N_4 based hydrogel showed a small peak at around 27.2^o which is characteristic of g-C_3N_4 while no such peaks appeared in the spectra of the blank hydrogel [28]. This further confirms the incorporation of g-C_3N_4 within the hydrogel.

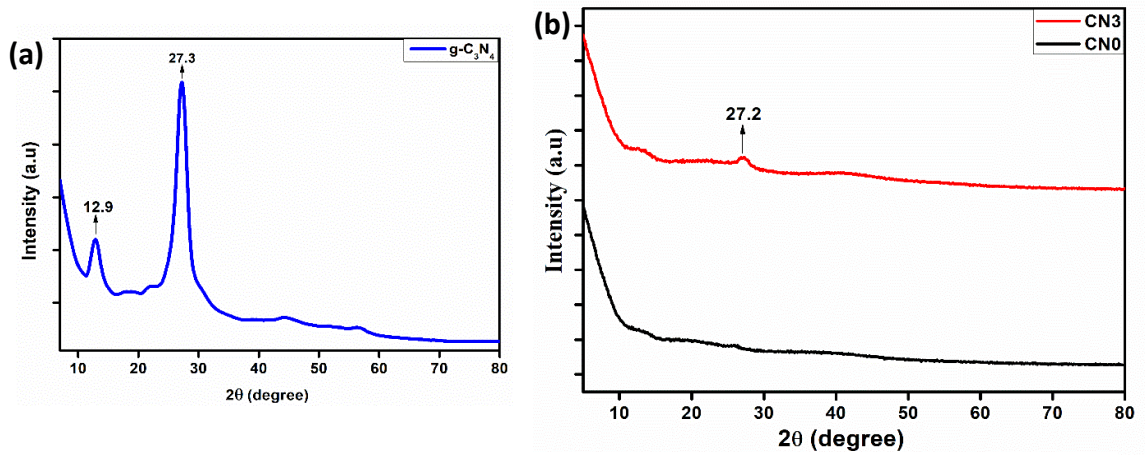

Figure 4.2 Powder X-ray diffraction pattern of (a) bulk g-C_3N_4, (b) CN hydrogel and blank hydrogel

4.4.4 SEM and TEM analysis

The morphological structure of the g-C_3N_4 as shown from the SEM image reveals disorderly stacked layers consisting of heterogeneously distributed and agglomerated structures which was further confirmed by its TEM images. From, the SEM images of the synthesized hydrogel, it was found that the blank hydrogel (CN0) appeared to have a smooth morphological surface. Whereas g-C_3N_4 with disorderly stacked layers when incorporated into the hydrogel matrix, turns the smooth surface of hydrogel into uneven and lamellar structures thereby revealing the successful incorporation of g-C_3N_4 into the hydrogel matrix. The SEM and TEM images are shown in Figure 4.3 (a),(b),(c), and (d)

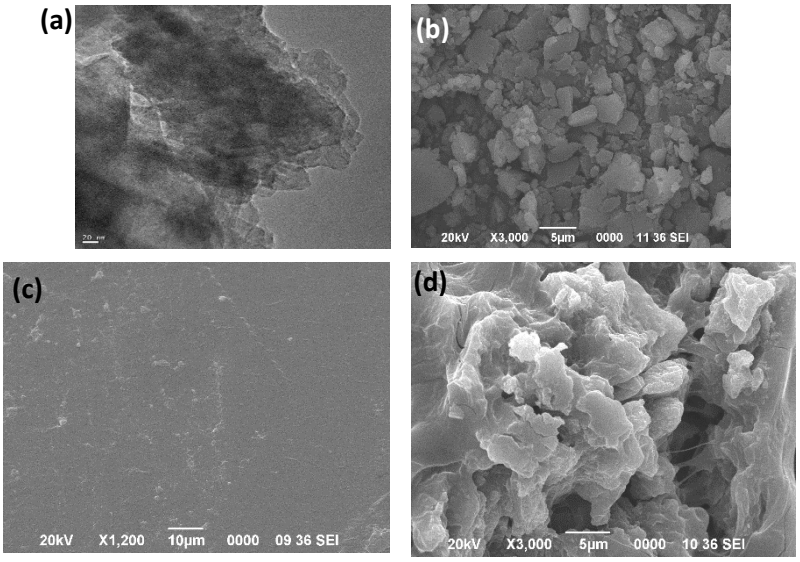

Figure 4.3 (a) TEM image of bulk g-C_3N_4 powder, SEM images of (b) bulk g-C_3N_4 powder, (c) CN0 hydrogel, (d) cross-section CN5 hydrogel

4.4.5 UV-Vis spectroscopy

The UV-visible absorbance of bulk g-C_3N_4, blank hydrogel (CN0), and CN5 hydrogel (hydrogel with 5wt% g-C_3N_4) were determined and shown in Figure 4.4. The optical band structure of g-C_3N_4 as characterised by UV-visible absorption spectroscopy shows strong absorption in the range of 250-550 nm which is like a typical semiconductor absorption spectrum. These absorptions are attributable to the π-π* or n-π* electronic transitions. The optical band gap of g-C_3N_4 was also calculated from the tauc plot and was found to be 2.66 eV. Comparing the absorbance of CN0 and CN5 hydrogel, it was found that CN5 hydrogel shows a significant hyperchromic shift which further confirms the incorporation of g-C_3N_4 into the hydrogel matrix. Although the absorption intensity of bulk g-C_3N_4 is stronger than that of CN5 hydrogel, the absorption ability of CN5 hydrogel in the visible region is much higher than that of bulk g-C_3N_4. This indicates that the incorporation of g-C_3N_4 into the hydrogel matrix broadened the absorption wavelength of bulk g-C_3N_4, resulting in the improved photocatalytic property of g-C_3N_4.

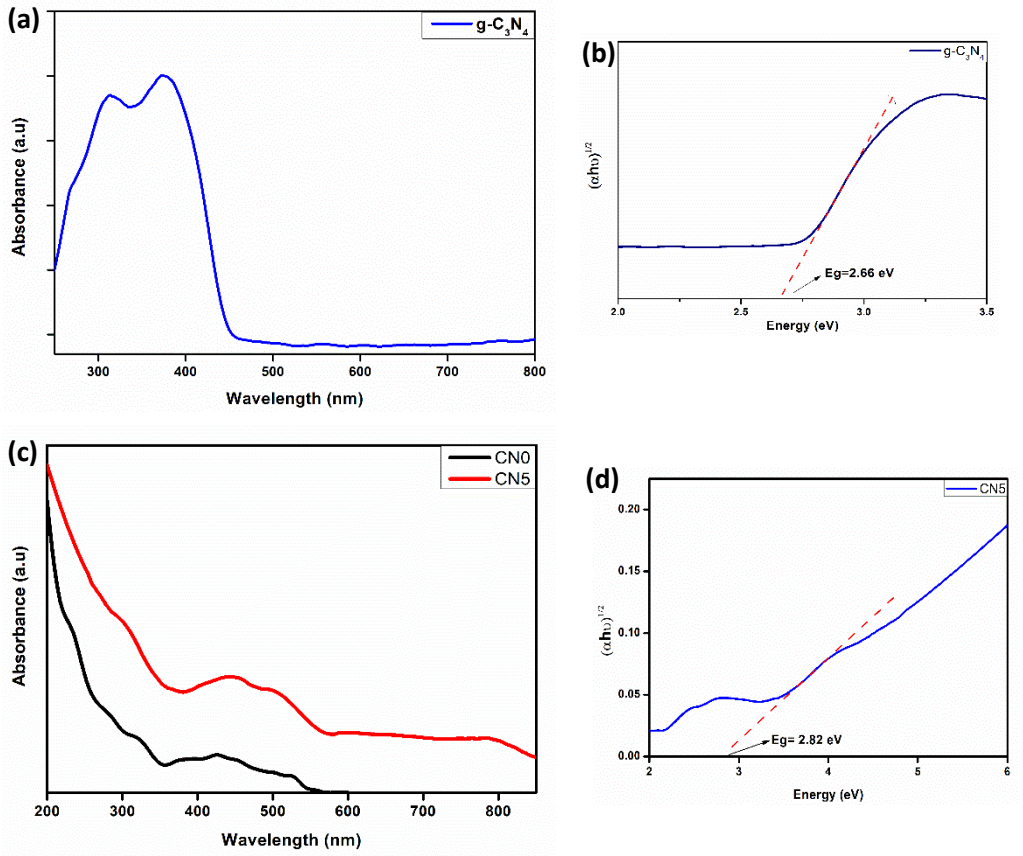

Figure 4.4 (a, c) UV-Visible absorbance spectra and (b, d) Band gap energy of the synthesized bulk g-C_3N_4, CN0, and CN5 hydrogel

4.4.6 CHN analysis

The CHN elemental analysis of CN0 and CN5 is shown in Table 4.2. The content of C and N atoms in CN5 hydrogel (with g-C_3N_4 incorporation) is comparatively higher than that in CN0 hydrogel (without g-C_3N_4). However, the change in the H atom in both the hydrogel is negligible. These results further confirmed the successful incorporation of g-C_3N_4 within the hydrogel matrix.

Table 4.2 Elemental composition of CN0 and CN5 hydrogel obtained from CHN analysis.

Sample	*C%*	*H%*	*N%*
CN0	37.68	7.15	10.11
CN5	40.29	7.04	13.54

4.4.7 PL spectroscopy

The steady-state PL spectra of the synthesized bulk g-C_3N_4, CN5 hydrogel and CN0 hydrogel are shown in Figure 4.5. The spectrum for bulk g-C_3N_4 showed a broad peak around 437 nm with an excitation of 375 nm which results from the strong radiative recombination of photogenerated electron-hole pairs. Again, the spectrum of CN0 hydrogel doesn't show any emission peak. However, the CN5 hydrogel shows a strong peak around 533 nm depicting the successful incorporation of g-C_3N_4 within the hydrogel matrix. Analysis of both the bulk g-C_3N_4 and CN5 hydrogel shows a progressive red shift with increasing emission intensity revealing the physical interaction between the hydrogel and bulk g-C_3N_4.

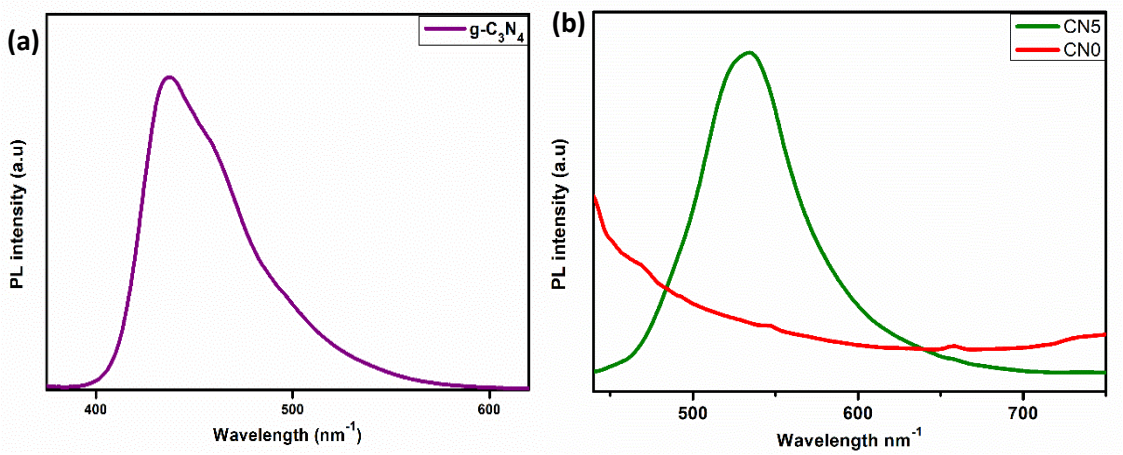

Figure 4.5 PL spectra of (a) bulk g-C_3N_4, (b) CN5 and CN0 hydrogel

4.4.8 TGA analysis

TGA results reveal that the synthesized hydrogel is relatively stable and can be used under an elevated range of temperatures. As shown in Figure 4.6, the initial weight loss of 8% between 90 °C to 230 °C is mainly attributed to the loss of moisture within the gel. The maximum weight loss of 39% occurs in the temperature range of 230 °C to 330 °C which might be due to the decomposition of the sulphonic and amide group. The final decomposition above 350 °C is probably due to the degradation of C-C bonds in the polymeric chain [40,41].

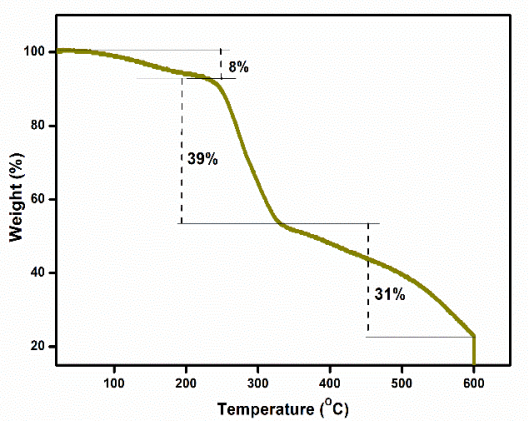

Figure 4.6 TGA spectra of CN5 hydrogel

4.4.9 Swelling behaviour

The swelling behaviour of the hydrogel is one of the important features of the hydrogel as it has significant impact on various applications, particularly when applied in water treatment. Therefore, by varying the content of g-C_3N_4 in the hydrogel, a series of experiments have been performed to determine the swelling behaviour of the hydrogel.

When the hydrogel was immersed in distilled water, it showed maximum swelling within an hour. However, to examine the equilibrium swelling, the hydrogels were immersed in water for 24 hours. In general, the addition of a reinforcing agent decreases the swelling behaviour of the hydrogel [42]. Therefore, it is difficult to maintain the swelling property while introducing a reinforcing agent into a hydrogel matrix. Here, we have found that on an aqueous solution (pH 7), the hydrogel with 5wt% g-C_3N_4 shows maximum swelling of 4783% without causing any degradation to the three-dimensional structure. This excellent swelling behaviour of the hydrogel can be attributed mostly to the presence of an ionizable sulfonate group within the hydrogel matrix causing high repulsion, thereby allowing water molecules to penetrate easily. Moreover, it was found that with the increase in the content of g-C_3N_4 from 1wt% - 5wt%, the swelling behaviour of the hydrogel increases. This enhanced water absorption property with increasing g-C_3N_4 content could be explained by the formation of a more porous structure with a high surface area and enhanced expansion capacity. Again, the overall swelling behaviour of the hydrogel in acidic conditions (HCl solution of pH 1) is lower compared to their swelling in basic conditions (NaOH solution of pH 10). This is because, in acidic conditions, most of the sulfonate group remains protonated thereby restricting electrostatic repulsion. The swelling behaviour of the hydrogel is shown in Fig 4.7.

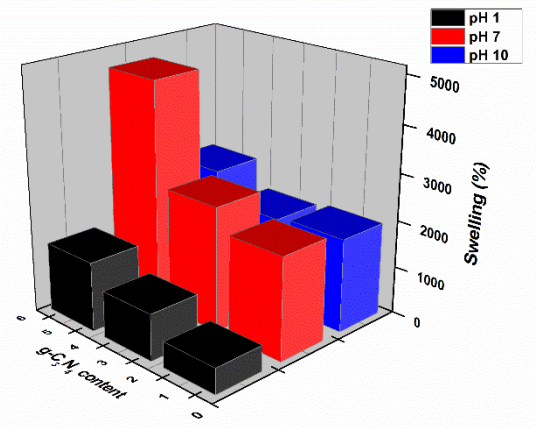

Figure 4.7 Swelling behaviour of the hydrogel at g-C_3N_4 concentration of 1wt%, 3wt% and 5wt% at pH values of 1, 7 and 10

4.4.10 Compressibility

The mechanical properties of the hydrogel can be studied by performing compression tests. It was found that the hydrogels with varying compositions of g-C_3N_4 exhibited high compressibility. The compressive stress-strain curve for the hydrogel with varying compositions of g-C_3N_4 has been shown in Fig 4.8 (a). However, the detailed value with Young's modulus is shown in Table 4.3.

It is seen that, when the hydrogels were compressed up to a strain of 100%, the hydrogels with 0.8wt% (CN0.8) and 1wt% g-C_3N_4 (CN1) content show the compressive strength of 0.12 MPa and 0.08 MPa. On further increasing the content of g-C_3N_4 to 2wt% and 5wt%, a slight reduction in the mechanical strength is observed and compressive strain decreases to 73% and 80% respectively. This might be due to the reason that on increasing the content of g-C_3N_4, the crosslinking density of the hydrogel becomes denser and less homogenous, resulting in the cracking of the hydrogel at lower strain. However, a remarkable change is observed in the CN3 (hydrogel with 3wt% g-C_3N_4), where it achieved an excellent mechanical strength of 0.55MPa and can be compressed up to a strain of 230% without cracking. The high compressibility of the hydrogel results from the increasing hydrogen bonding between the polymer chain and the g-C_3N_4 layers. The additional crosslinking induced by g-C_3N_4 into the hydrogel increases its mechanical properties.

The cyclic compressibility of the CN3 hydrogel is shown in Figure 4b. During the experiment, the hydrogel was compressed to a strain of 80% and was recovered to its original state rapidly without causing any cracking or damage even after 20 cycles. The mechanical strength of 0.07MPa is also retained after 20 cycles. The repetitive

compression cycle is shown in Figure 4.8(b). Alongside, the flexibility of the hydrogel can be seen from its resistance towards sharp objects. For example, when a piece of hydrogel is compressed with a sharp blade (Figure 4.8(c)), it shows resistivity and remains undamaged even after multiple compression. This again determines the strength of the network within the hydrogel.

Table 4.3 Compressive stress along with strain and Young's modulus are shown with varying compositions of g-C_3N_4

Composition (wt% of total monomer)	*Stress (MPa)*	*Strain*	*Young's modulus (KPa)*
0.8	0.12	100	1.2
1	0.08	100	0.8
2	0.09	73	1.232877
3	0.55	230	2.391304
5	0.07	80	0.875

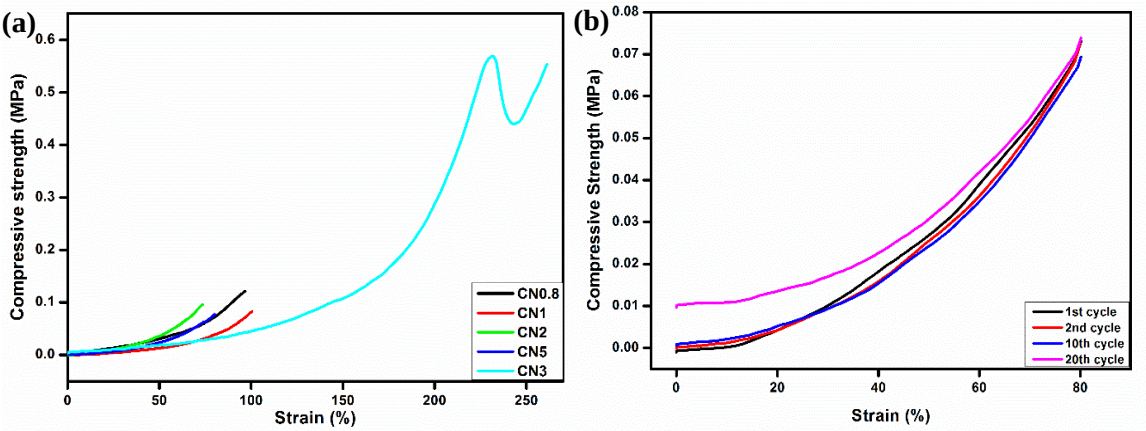

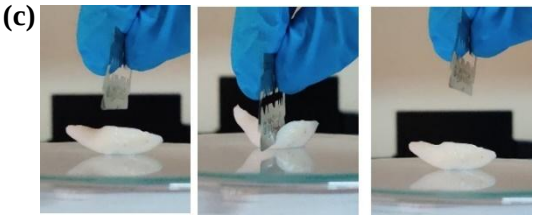

Figure 4.8 (a) Compressive strength of the CN hydrogel by varying the composition of g-C_3N_4, and (b) Repetitive compressive strength of the hydrogel by performing various cycle, and (c) Digital photograph of the hydrogel when compressed with a sharp object

4.4.11 Removal of organic dye by the synergistic effect of adsorption and photocatalytic degradation

The removal of cationic CV dye by the CN hydrogel is hypothesized to be removed from the solution by the synergistic effect of adsorption and photocatalytic degradation. Therefore, to determine the contribution of each removal mechanism, different experiments were performed by considering two conditions (i) with hydrogel under dark conditions and (ii) with hydrogel under visible light irradiation.

Using a UV-visible absorbance spectrophotometer, the dye concentration was measured at an interval of 30 min over a definite time. From Figure 4.9(d), it is seen that for over 210 min, the dye removal efficiency of the hydrogel under dark conditions is only 29% which is many times lower compared to the hydrogel under light irradiation where within 210 min, it shows dye removal efficiency of 90% when put under visible light. Moreover, even after 1260 min (21 h), the hydrogel could not completely remove the dye under dark conditions. Therefore, these findings supported the above hypothesis that removal of the dye is due to the conjoining effect of both adsorption and degradation mechanism where the dye molecule first adsorbed into the hydrogel matrix followed by degradation *via* g-C_3N_4 mediated photocatalysis. The rapid removal of the dye upon the addition of hydrogel into the dye solution can be attributed to the highly porous structure of the hydrogel which allows easy diffusion of the organic dye molecule through the gel to the photocatalytic site. In addition, the electrostatic interaction between the negatively charged hydrogel matrix and the positive charge on the CV molecule accelerates the adsorption of the dye molecule resulting in rapid removal of dye. The UV-visible absorption spectra of CV dye on treatment with hydrogel under light irradiation and dark conditions are shown in Figure 4.9(a) and(b).

Pure bulk g-C_3N_4 also exhibits photocatalytic properties towards dye degradation. However, the efficiency of photodegradation of pure g-C_3N_4 is much lesser compared to the g-C_3N_4-hydrogel composites. In a controlled experiment, a comparative analysis was performed for a definite time to determine the photodegradation efficiency of bulk g-C_3N_4 and CN hydrogel under visible light irradiation. For this, 0.09 g of bulk g-C_3N_4 was used whereas the 0.09 g hydrogel used contained only 0.03 g of g-C_3N_4. It was found that the dye degradation efficiency of bulk g-C_3N_4 is 80% less compared to the degradation efficiency of CN hydrogel when studied for 180 min. This limited photocatalytic property of pure g-C_3N_4 is due to its poor dispersibility which causes its

agglomeration, poor adsorption ability, and small specific surface area. Therefore, the dye molecules could not approach the surface of g-C_3N_4 hence no effective photodegradation takes place. On the other hand, after the incorporation of g-C_3N_4 into the hydrogel matrix, no agglomeration of g-C_3N_4 occurs. The g-C_3N_4 in the hydrogel retains its photocatalytic property which further serves its purpose in degrading organic dyes. After illuminating light, the g-C_3N_4 on the hydrogel matrix generates couples of e^- and h^+ which further generate $^{\cdot}O_2^-$ and OH^- thereby degrading the organic pollutant to produce CO_2 and H_2O as byproduct. Moreover, the high hydrophilic property of hydrogel allows easy and fast adsorption of dye molecules which facilitates effective photodegradation over the surface of g-C_3N_4 particles. The graphical representation of the mechanism of dye removal by the hydrogel is shown in Figure 4.10. The UV-visible absorbance spectra of dye treated with pure g-C_3N_4 and CN3 (hydrogel with 3wt% of g-C_3N_4) are shown in Figure 4.9(c)

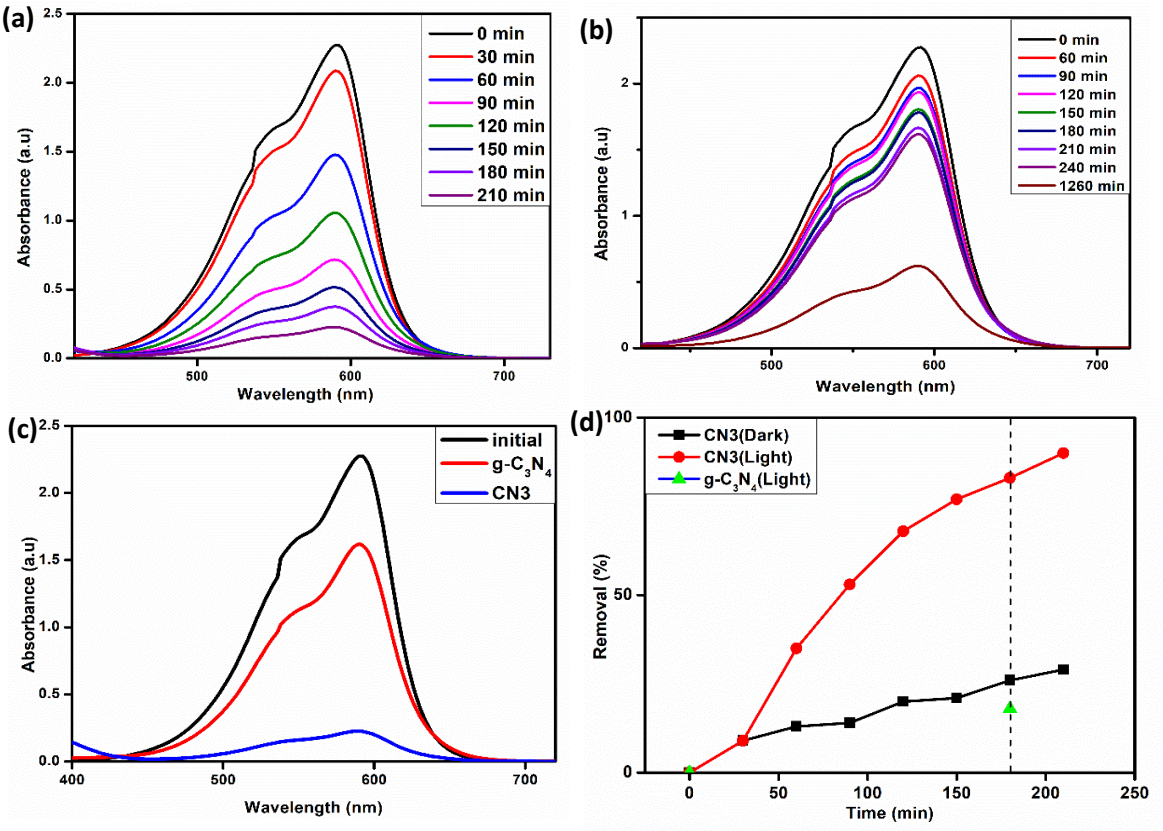

Figure 4.9 UV-Visible absorbance spectra of the dye treated (a) with hydrogel under light irradiation, (b) with hydrogel under dark condition, (c) with hydrogel, g-C_3N_4 powder for a definite time, (d) Relative removal efficiencies of the dye by the hydrogel as a function of irradiation time under different light condition

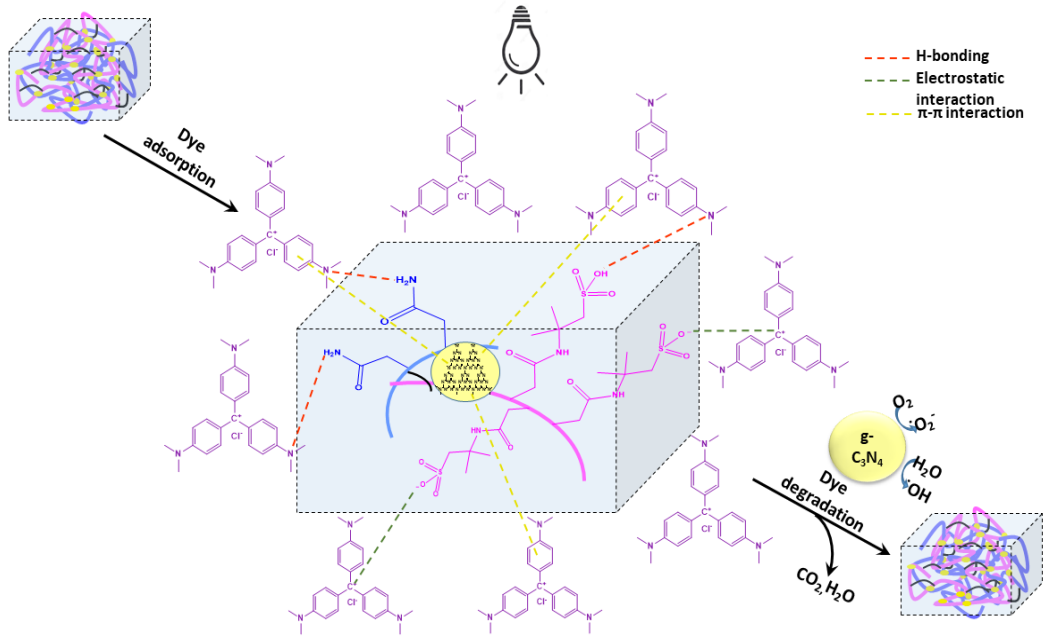

Figure 4.10 Graphical representation of the mechanism of dye removal by the hydrogel

4.4.11.1 Effect of g-C_3N_4 content on dye removal

At a definite interval of 150 min, it was found that hydrogel with g-C_3N_4 content of 1wt% shows a maximum dye removal of 98%. However, increasing the content of g-C_3N_4 from 1wt% to 4wt%, there is a lowering in dye removal efficiency. This can be attributed to the additional electrostatic interaction between the dye molecule and the negatively charged electron cloud of g-C_3N_4 on the surface of the hydrogel. This interaction slackens the penetration of dye molecules within the hydrogel matrix, thereby lowering the removal efficiency. The dye removal efficiency of the hydrogel with different g-C_3N_4 is shown in Figure 4.11.

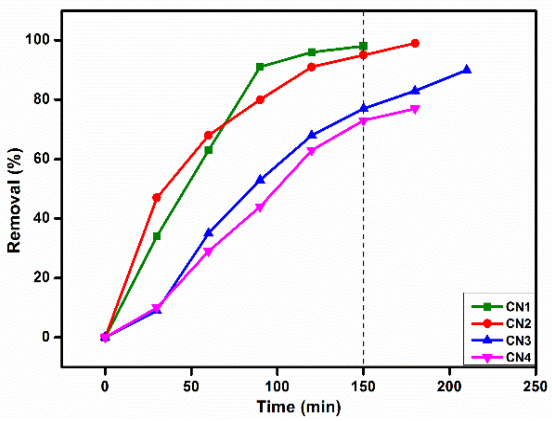

Figure 4.11 Relative removal efficiencies of the dye by the hydrogel as a function of irradiation time under varying content of g-C_3N_4,

4.4.11.2 Effect of pH on dye removal

As seen in Figure 4.12, the overall dye removal efficiency of the hydrogel at acidic, neutral, and basic pH solutions is almost equivalent. However, there is a slight decrease in the removal efficiency at pH 1. These changes in removal efficiency are due to the protonation of the ionisable group within the hydrogel moiety at an acidic solution (pH 1), which decreases the electrostatic interaction between the cationic group in the dye molecule and the anionic group in the hydrogel moiety, thereby lowering the dye adsorption and consequently lowers the degradation.

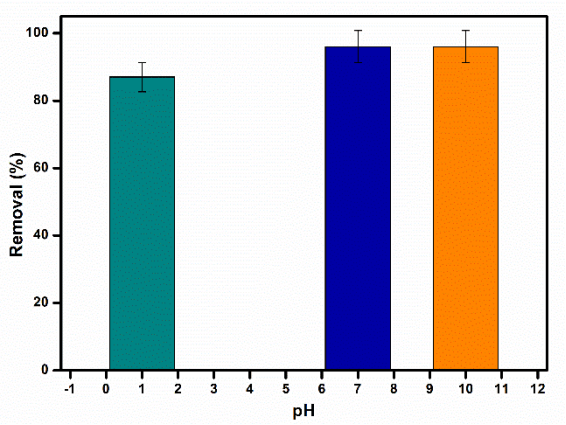

Figure 4.12 Dye removal efficiency of the hydrogel at pH 1, pH 7, and pH 10

4.4.11.3 Kinetic studies of dye degradation

The kinetics of dye degradation towards CV dye was determined by plotting pseudo-first order and pseudo-second order kinetic model and their corresponding mathematical equation are given below:

$$ln\left(\frac{C_0}{C_t}\right) = k_1 t \quad (1)$$

$$\frac{1}{C_t} = \frac{1}{C_0} + k_2 t \quad (2)$$

Where C_o, C_t are the initial concentration and concentration at time t respectively, k_1 and k_2 are the rate constant for pseudo-first order and pseudo-second order respectively.

Figure 4.13 (a) and (b) represent the graph between $\ln(C_o/C_t)$ *vs* time for pseudo-first order and $1/C_t$ *vs* time for pseudo-second order. It is seen that the plot for pseudo-first order fitted best with a correlation coefficient (R^2) of 0.99. Therefore, the

photodegradation of CV dye by the hydrogel is considered to follow the pseudo-first-order kinetic model.

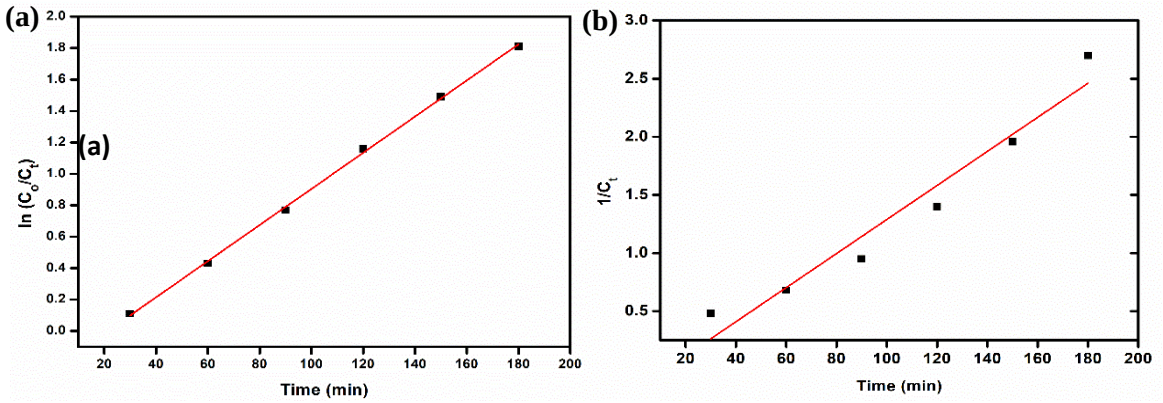

Figure 4.13 Fit plot of (a) pseudo-first order, (b) pseudo-second-order kinetics model for dye degradation

4.4.11.4 Scavenger test

The photocatalytic degradation of organic dyes generally involves many reactive species such as hydroxyl radical ($^{\cdot}OH$), superoxide radical ($^{\cdot}O_2^-$), holes (h^+), and electrons (e^-). Therefore, to determine the role of different reactive species responsible for the degradation of CV dyes, reactive species trapping experiments were performed using a series of scavengers such as ethylenediamine tetraacetic acid (EDTA) for h^+, isopropanol (IPA) for $^{\cdot}OH$, benzoquinone (BQ) for ($^{\cdot}O_2^-$), and potassium persulphate ($K_2S_2O_8$) for e^- [43-46]. The degradation efficiency of the hydrogel as shown in Figure 4.14 demonstrates that the addition of BQ had a significant impact on degradation by minimizing the removal efficiency to 48%. Alongside, the addition of IPA and $K_2S_2O_8$ decreases the removal efficiency to 72% and 78% respectively. The addition of BQ shows the highest impact on the degradation reaction suggesting that the effect of superoxide ion is higher relative to the other reactive species.

The mechanism of photodegradation of dyes has been broadly discussed in the literature and can be generalized into steps as shown below:

$$CN \longrightarrow CN + e^- + h^+$$

$$e^- + O_2 \longrightarrow {}^{\cdot}O_2^-$$

$$h^+ + H_2O \longrightarrow {}^{\cdot}OH + h^+$$

$$CV + h^+ \longrightarrow \text{oxidation product}$$

$$CV + e\text{-} \longrightarrow \text{reduction product}$$

Here, the hydrophilic nature of hydrogel allows the dye molecules to come closer to the surface of g-C_3N_4. On light irradiation, the photoelectrons from the filled valence band are promoted to the empty conduction band thereby generating e^- and h^+ pair. This e^-/h^+ pair can also directly react with the dye molecule. The highly reactive radical species thus formed react with the dye molecule to give water and carbon dioxide as degraded products.

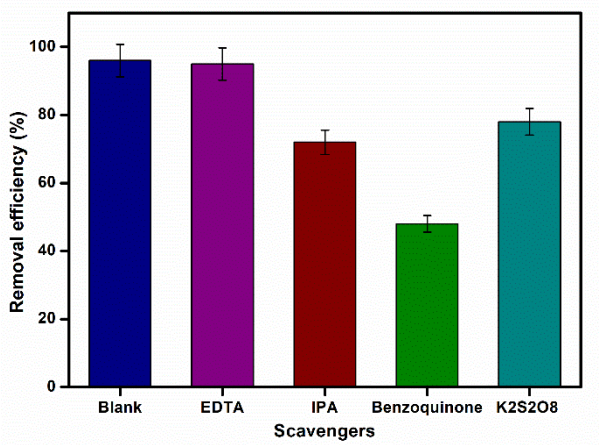

Figure 4.14 Dye removal efficiency of the hydrogel under the influence of different scavengers

4.4.11.5 Selective behaviour to dyes

The behaviour of the hydrogel to different dyes was further determined by qualitative analysis of the hydrogel on different cationic dyes such as RhB, and MB as well as on anionic dye MO. The results as shown in Figure 4.15(a), (b), and (c) demonstrate that the hydrogel degrades both the cationic dyes rapidly within 150 min. However, it fails to degrade the anionic dye methyl orange. These results indicate that for the dyes to be adsorbed and degraded by the hydrogel, there must be a strong interaction between the hydrogel matrix and the dye molecules. Since the overall charge possessed by hydrogel is negative because of the presence of the sulphonic group, it can easily form an electrostatic interaction with positively charged dye and thereby efficiently remove the cationic dye. However, it fails to remove anionic dye as there no such interaction takes place.

The degradation efficiencies of the hydrogels towards both cationic dyes have been shown in Figure 4.15(d). On light irradiation, for a period of 150 min, the hydrogel shows removal efficiencies of 97% and 92% towards MB and RhB dyes respectively.

To further validate the selectivity of the hydrogel towards cationic and anionic dyes, the hydrogel was allowed to treat a mixture of dyes containing cationic CV and anionic MO, and the results support the above explanation. (Figure 4.15(e)). The digital photographic images are shown in Figure 4.15(f).

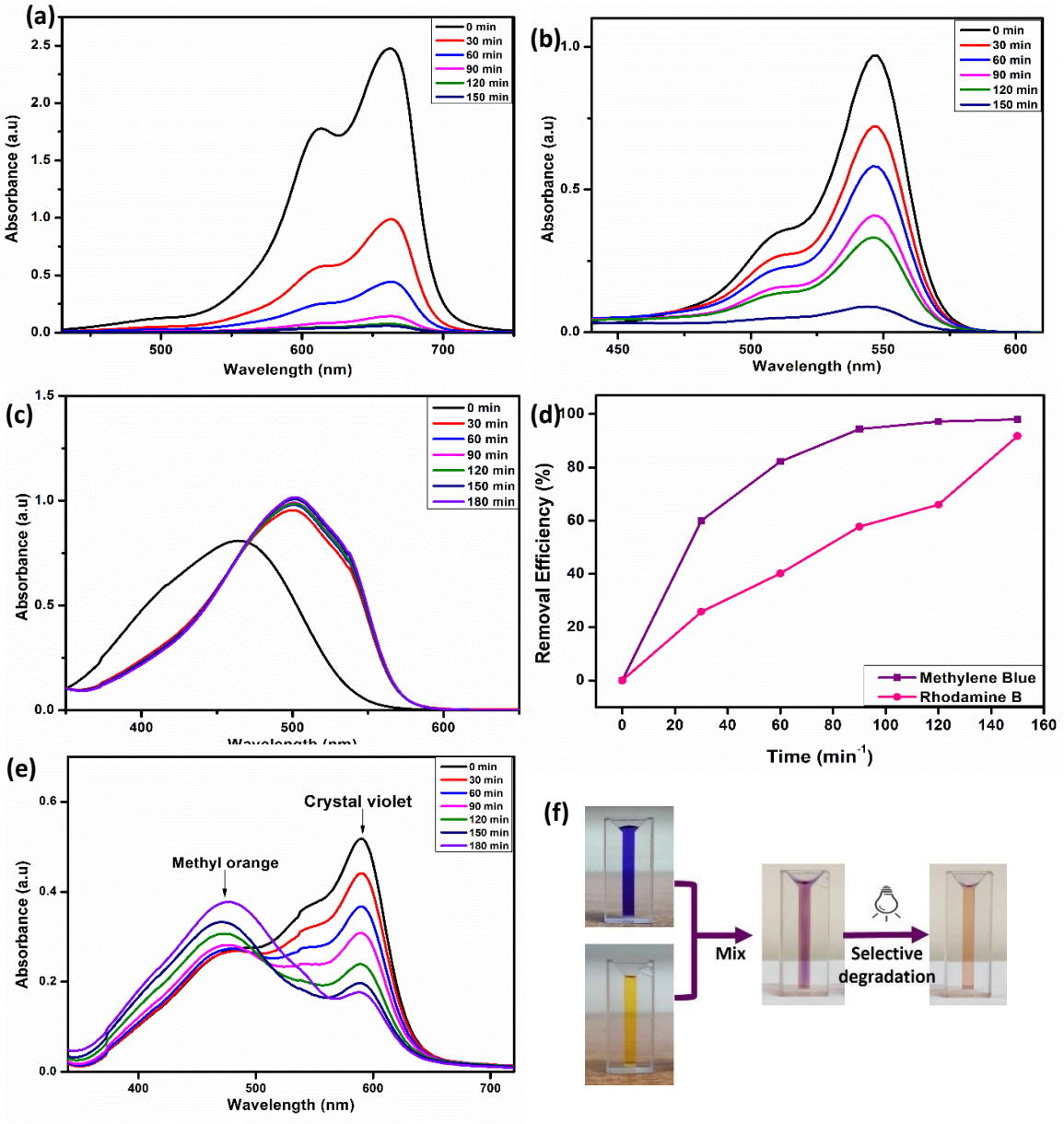

Figure 4.15 UV-Vis absorbance spectra showing removal of (a) MB dye, (b) RhB dye, (c) MO dye, (d) Removal efficiency of hydrogel towards MB and CV dyes, (e) UV-Vis absorbance spectra showing removal of mix dye of CV/MO under light irradiation at different time intervals, and (f) Digital image showing selective degradation performance by hydrogel from a CV/MO mix dye solution

4.4.12 Recyclability

The reusability of the CN hydrogel was determined by performing 5 consecutive cycles. As shown in Figure 4.16(a), there is no loss in removal efficiency even in the 5th cycle. However, the change in removal efficiency after the 1st cycle demonstrates the breakdown of the hydrogel to small hydrogel particles on dye diffusion. These small particles offer more surface area for the dye molecule to be adsorbed and degraded, thereby increasing the removal efficiency.

The characterization of the CN hydrogel after recycling was carried out. As shown in Figure 4.16(b), FTIR spectra of the CN hydrogel after the 5th cycle showed no appreciable change. However, there is a small decrease in intensity in the range of 1250 cm^{-1} to 1150 cm^{-1}. This decrease in intensity around 1250 cm^{-1} is due to the electrostatic interaction of the C-N group of the hydrogel with residual CV dye molecules. Similarly, the decreasing intensity around 1170cm^{-1} is due to the interaction of the -SO_3 group of hydrogels with the CV dye molecules. The small peak at 809cm^{-1} depicts the presence of g-C_3N_4 in the dye-treated hydrogel. Again, from the SEM morphology of the hydrogel after the 5th cycle demonstrates a nonporous and smooth wavy surface which is due to the subsequent drying and swelling process that causes a change in morphology on the hydrogel surface (Figure 4.16(c). Therefore, the above results indicate that, although the hydrogel shows recyclability up to 5 cycles, a small portion of residual dye molecules got adsorbed within the hydrogel matrix thereby causing small changes in the structure and morphology of the dye-treated hydrogel.

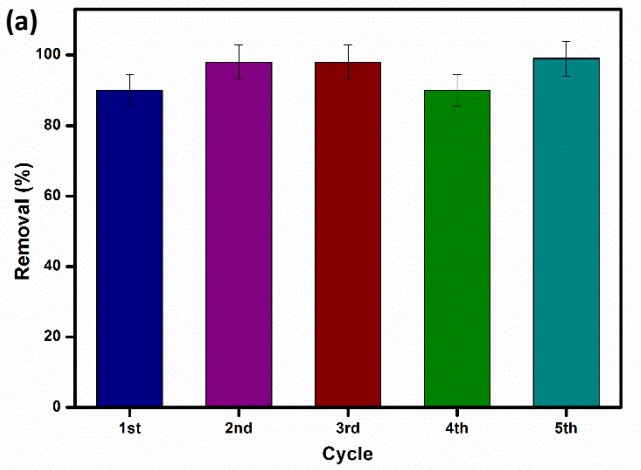

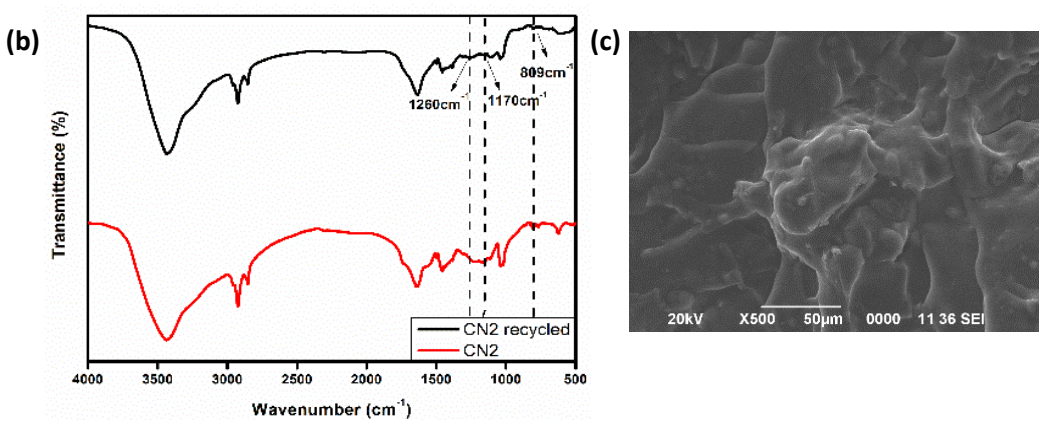

Figure 4.16 (a) Repeatable removal efficiency of the hydrogel up to 5 cycles (b) FTIR spectra of the hydrogel before and after recycling and (b) SEM morphology of the hydrogel after recycling

4.4.13 Adsorption property of the hydrogel towards the dye

To investigate the adsorption property of the synthesized hydrogel, we have chosen CV dye as a model dye. We have studied the effect of adsorbent dosage, initial concentration, and contact time on the removal efficiency and adsorption capacity of the hydrogel.

4.4.13.1 Effect of adsorbent dosage

The effect of adsorbent dosage on dye adsorption is determined by immersing different dosages of adsorbent into a dye solution of 30 ml with a concentration of 10 ppm until the attainment of equilibrium adsorption. As shown in Figure 4.17, at equilibrium, the removal efficiency of all the adsorbents with different dosages are same *i.e.* around 98%. However, with an increase in adsorbent dosage from 25 mg to 100 mg, the adsorption capacity (q_e) decreases. This change can be attributed to the reason that as the mass of the adsorbent increases, the number of adsorbates adsorbed per unit weight of adsorbent decreases, resulting in a decrease in the q_e value with increasing adsorbent mass. Thus, these results suggested that 25mg of the synthesized hydrogel is sufficient for adsorbing 30 ml of 10 ppm CV dye solution.

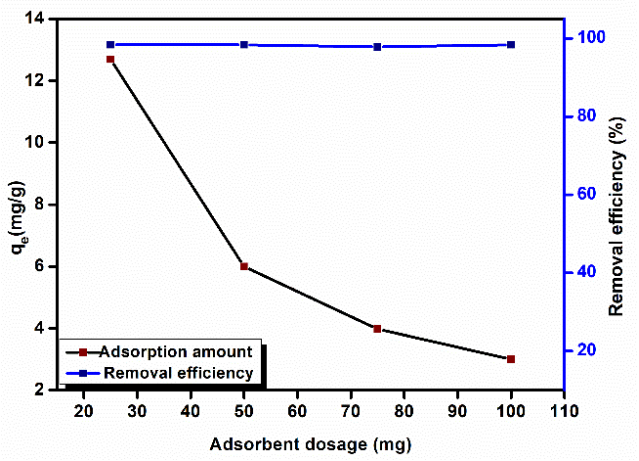

Figure 4.17 Effect on adsorption amount and removal efficiency of CV dye by the CN3 hydrogel with different adsorbent dosage

4.4.13.2 Effect of contact time

The effect of contact time was determined from the adsorption capacity and removal efficiency of the hydrogel towards CV dye by immersing 100mg of the adsorbent to a 30 ml dye solution of 10 ppm concentration. The adsorption amount and removal efficiency at time t were plotted against time (t, h) as shown in Figure 4.18. The rate of adsorption is the highest in the initial state however with time, rate of adsorption gradually decreases and finally reaches the equilibrium. Therefore, initially, there must occur some electrostatic interaction between active sites on the hydrogel and the dye molecules. After the occupation of all the active sites, there might occur only diffusion of small dye molecules into the porous structure of the hydrogel matrix resulting in a decline in the rate of dye adsorption.

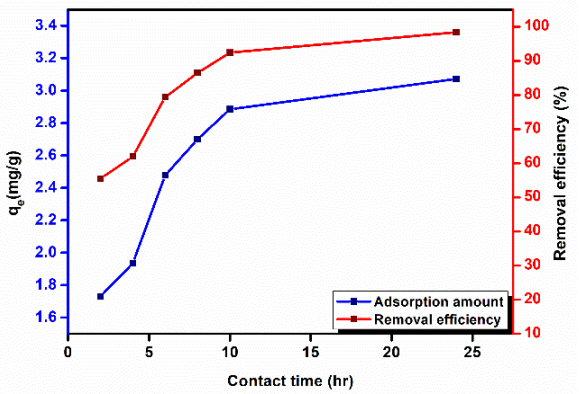

Figure 4.18 Effect on adsorption amount and removal efficiency of CV dye by the CN3 hydrogel at different contact time

4.4.13.3 Effect of initial concentration

To evaluate the effect of initial concentration on dye adsorption, 0.03g of adsorbent was immersed into a 50 ml of CV dye solution with different concentrations of 5 ppm to 50 ppm. From Figure 4.19 (a), it is seen that the dye adsorption capacity is dependent on the initial dye concentration which shows that with an increase in dye concentration, adsorption amount increases. This is due to the increased driving force of the concentration gradient causing increased adsorption on the adsorbents. However, the removal efficiency at the equilibrium is around 99% for all the different concentrations of dye. In general, it is found that with the increase in the initial concentration of dye, there is a decline in dye removal efficiency. This accounts for the saturation of adsorption sites as well as saturation in diffusion [47]. But here we found no such decrease in removal efficiency with an increase in initial concentration implying that the hydrogel adsorbate has enough active sites to adsorb more dye molecules [48,49].

In addition, the adsorption capacity of the hydrogel towards MB and RhB has also been determined by varying the initial concentration of dyes. From Figure 4.19 (b) and (c), it is seen that similar to CV dyes, the adsorption capacity of both MB and RhB depends on the initial concentration of dyes. With the increase in dye concentration, the adsorption amount increases which is again due to the increased driving force of the concentration gradient that causes increased adsorption on the adsorbents. The removal efficiency of both the dyes at equilibrium for all the concentration of dyes is around 99%

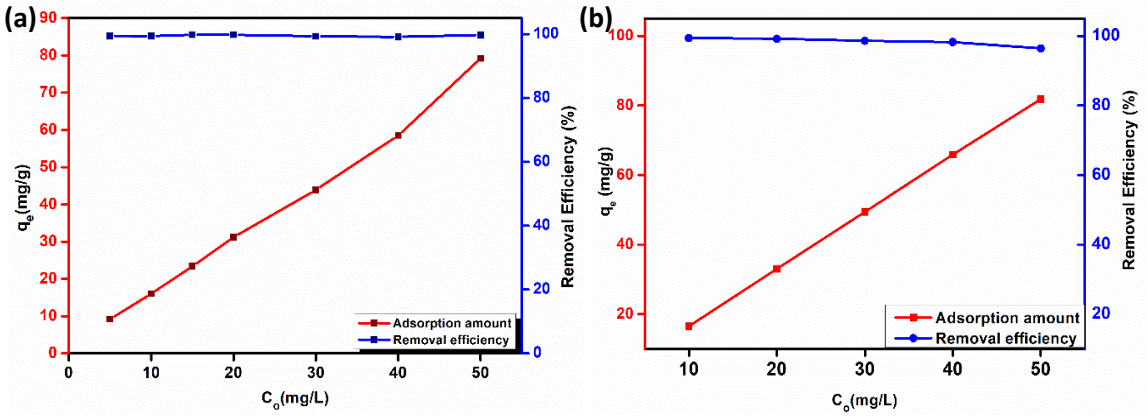

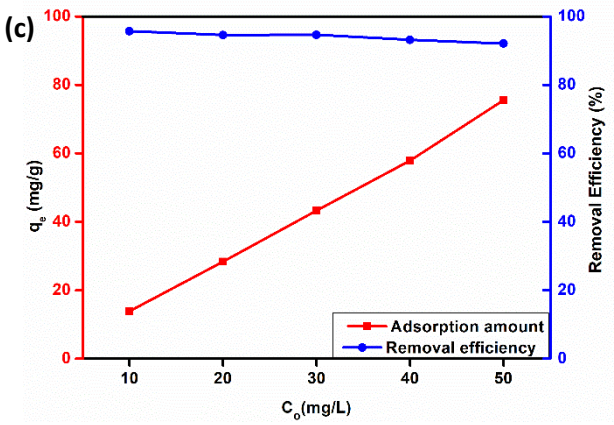

Figure 4.19 Effect on adsorption amount and removal efficiency of CV dye by the CN3 hydrogel with different initial concentration of (a) CV, (b) MB, and (c) RhB dyes

4.4.13.4 Adsorption isotherm

To analyse the adsorption mechanism of the synthesized hydrogel towards CV dye, Langmuir and Freundlich isotherm models were applied. Their corresponding mathematical equations are given below:

$$\frac{C_e}{q_e} = \frac{1}{q_m k_L} + \frac{C_e}{q_e} \quad (3)$$

$$\ln q_e = \ln k_F + \frac{1}{n} \ln C_e \quad (4)$$

Where C_e (mg/L) denotes the concentration of the solution at equilibrium, q_e (mg/g) is the adsorption amount at equilibrium, q_m is the maximum adsorption capacity, k_L and k_F represent the Langmuir and Freundlich isotherm constants respectively, n is the Freundlich constant which relates to the adsorption intensity. The adsorption isotherm curves plotted between C_e/q_e *vs* C_e (Langmuir) and ln q_e *vs* ln C_e (Freundlich) are shown in Figure 4.20(a) and (b) and their relevant fitting parameters are shown in Table 4.4. It was found that the correlation coefficient $R^2 > 0.99$ in the case of Langmuir which is close to 1 compared to Freundlich where R^2 differs from unity, thereby depicting that the adsorption of dye follows the Langmuir isotherm model. This indicates the formation of a monolayer by the dye molecule on the surface of the adsorbate.

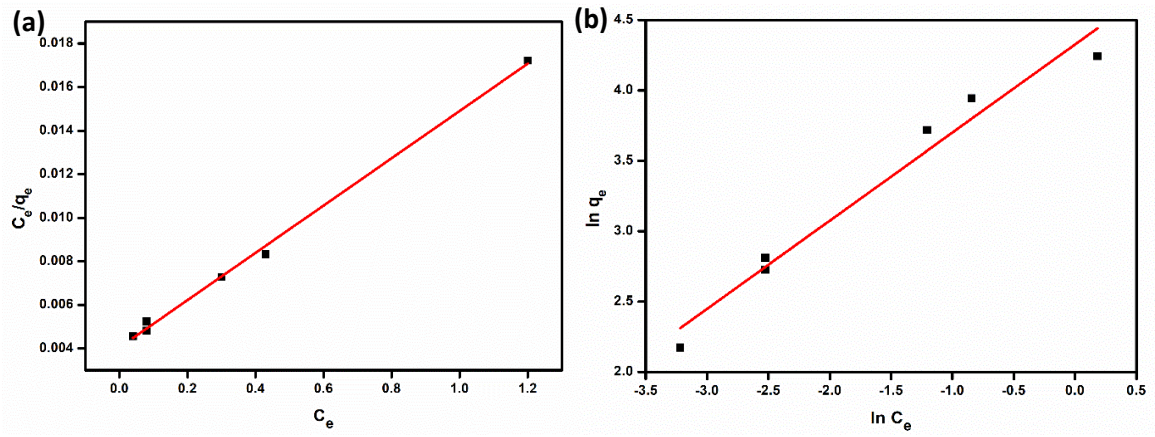

Figure 4.20 Linear fit plot of (a) Langmuir adsorption isotherm, (b) Freundlich adsorption isotherm model for adsorption of CV dye by the CN hydrogel

Table 4.4 Isotherm parameters for adsorption of CV dye by CN hydrogel

Models	*Parameters*	
Langmuir	q_{max} (mg/g)	100
	K_L (Lmg^{-1})	2.5
	R^2	0.996
Freundlich	1/n	0.626
	K_F	75.18
	R^2	0.96

4.4.13.5 Kinetic studies of dye adsorption

To investigate the adsorption kinetics, pseudo-first order and pseudo-second-order kinetics model were applied, and their corresponding mathematical expressions are given below:

$$\log(q_e - q_t) = \log q_e - \frac{k't}{2.303} \quad (5)$$

$$\frac{t}{q_t} = \frac{t}{q_e} + \frac{1}{k''q_e^2} \quad (6)$$

Where q_e (mg/g) is the adsorption capacity at equilibrium, q_t (mg/g) is the adsorption capacity at a specific time, t is time (h), k' (1/h) and k'' (g/mg.h) are the rate constants of pseudo-first order and pseudo-second order respectively. A graph between log (q_e-q_t) *vs* t for pseudo-first-order and t/q_t *vs* t for pseudo-second-order was plotted (Figure 4.21(a) and (b)). Their corresponding fitting plot reveals that the adsorption kinetics strongly

follow the pseudo-second-order kinetic model with a correlation co-efficient, $R^2 > 0.99$. The fitting parameters for both models are shown in Table 4.5.

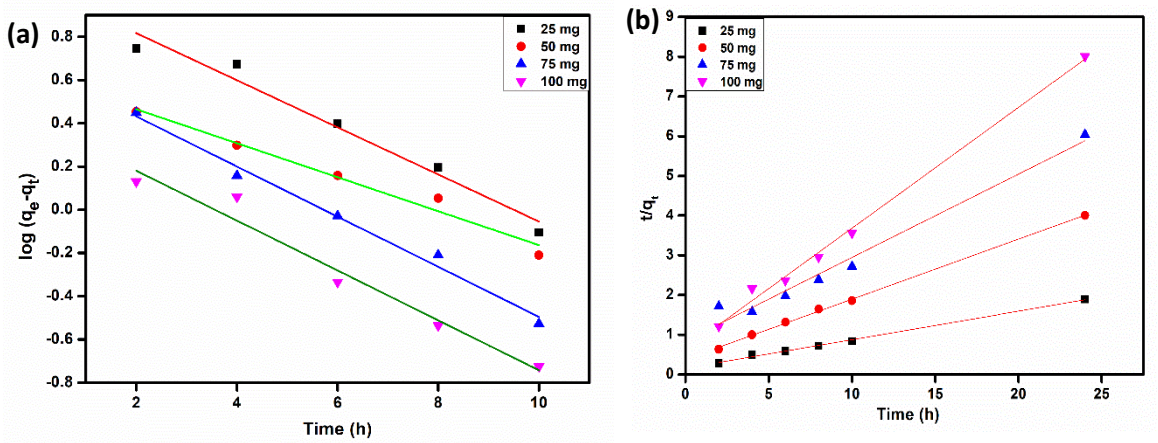

Figure 4.21 Fit plot for (a) Pseudo-first order and (b) Pseudo-second order kinetics for adsorption of CV dye by CN hydrogel with different adsorbent dosage

Table 4.5 Kinetic parameters for adsorption of CV dyes by CN hydrogel with different adsorbent dosage

Adsorbent dosage (mg)	q_e *(exp.) (mg/g)*	*Kinetic model*					
		Pseudo-first order			**Pseudo-second order**		
		k_1 (g/mg.h)	**q_e, (cal) (mg/g)**	**R^2**	**k_2 (g/mg.h)**	**q_e (cal) (mg/g)**	**R^2**
25	12.18	0.25	10.89	0.960	0.03	13.94	0.995
50	6.09	0.18	4.18	0.968	0.059	6.61	0.998
75	4.03	0.267	4.61	0.985	0.052	4.76	0.970
100	3.04	0.265	2.57	0.955	0.144	3.28	0.994

4.5 Conclusion

In this Chapter, we have successfully developed a facile one-pot synthesis method for the co-polymerization of AAm and AMPS monomer into a highly photoactive hydrogel. The developed hydrogel possesses good mechanical properties with high compressibility and swellable properties. Here, the excellent performance of g-C_3N_4 provides an efficient and eco-friendly photopolymerization technique. Moreover, after polymerization, the g-C_3N_4 retains its photocatalytic property within the hydrogel. This photocatalytic property of the hydrogel was further utilized to treat wastewater containing organic dyes. The well-defined porous structure of the hydrogel allows easy

and fast diffusion of organic molecules within the hydrogel matrix and the high surface area provides more active sites for the absorption of visible light thereby increasing the photocatalytic activity. Moreover, the hydrogel also shows good adsorption properties. Thus, the synergistic effect of adsorption and degradation by the hydrogel results in the rapid removal of organic dyes from the solution. The hydrogel allows easy handling and can be readily recovered from the solution without causing secondary pollution. The synthesized hydrogel can be reusable for up to 5 cycles with adequate removal efficiencies. The hydrogel also shows good adsorption behavior towards cationic dyes. Moreover, the excellent swelling capacity, as well as the high adsorption behavior shown by the hydrogel, highlights its applications as a superabsorbent for the removal of metal ions, pharmaceutical products, and other trace organic compounds from water bodies. In addition, the presence of photoluminescence property in the synthesized hydrogel offers new prospects in the field of sensors as a metal ion detector in water systems. Alongside this, the appreciable photocatalytic properties of the synthesized hydrogel also give new insight into its probable application in photocatalytic metal ion reduction. Thus, the work in this chapter provides a sustainable method for both photopolymerization and removal of toxic dyes thereby promoting their practical applications in waste-water treatment and other photocatalytic remediation.

References

[1] Zhao, X. Designing toughness and strength for soft materials. *Proceedings of the National Academy of Sciences*, 114(31):8138-8140, 2017.

[2] Panteli, P.A. and Patrickios, C.S. Multiply interpenetrating polymer networks: Preparation, mechanical properties, and applications. *Gels*, 5(3):36, 2019.

[3] Hu, L., Chee, P.L., Sugiarto, S., Yu, Y., Shi, C., Yan, R., Yao, Z., Shi, X., Zhi, J., Kai, D. and Yu, H.D. Hydrogel-based flexible electronics. *Advanced Materials*, 35(14):2205326, 2023.

[4] Sun, A., He, X., Ji, X., Hu, D., Pan, M., Zhang, L. and Qian, Z. Current research progress of photopolymerized hydrogels in tissue engineering. *Chinese Chemical Letters*, 32(7):2117-2126, 2021.

[5] Dhiman, A., Sharma, A.K. and Agrawal, G. Polymer based engineered materials for sustainable agriculture. *ACS Agricultural Science & Technology*, 2(4):693-711, 2022.

[6] Pu, J., Zhou, J., Chen, Y. and Bai, B. Development of thermotransformable controlled hydrogel for enhancing oil recovery. *Energy & Fuels*, 31(12):13600-13609, 2017.

[7] Li, J., Wang, Y. and Yue, Y. A Transparent, High-Strength, and Recyclable Core–Shell Structured Wood Hydrogel Integrated with Carbon Dots for Photodegradation of Rhodamine B. *ACS Applied Nano Materials*, 6(4):2894-2907, 2023.

[8] Nayak, S., Prasad, S.R., Mandal, D. and Das, P. Carbon dot cross-linked polyvinylpyrrolidone hybrid hydrogel for simultaneous dye adsorption, photodegradation and bacterial elimination from waste water. *Journal of hazardous materials*, 392:122287, 2020.

[9] Kumru, B., Molinari, V., Shalom, M., Antonietti, M. and Schmidt, B.V. Tough high modulus hydrogels derived from carbon-nitride *via* an ethylene glycol co-solvent route. *Soft Matter*, 14(14):2655-2664, 2018.

[10] Liu, J., An, T., Chen, Z., Wang, Z., Zhou, H., Fan, T., Zhang, D. and Antonietti, M. Carbon nitride nanosheets as visible light photocatalytic initiators and crosslinkers for hydrogels with thermoresponsive turbidity. *Journal of Materials Chemistry A*, 5(19):8933-8938, 2017.

[11] Parhizkar, J. and Mohammad Shafiee, M.R. Hydrogel Based Nanocomposite Photocatalyst Containing In_2S_3/g-C_3N_4 for Removal of Dye from Water. *Nanochemistry Research*, 5(2):168-178, 2020.

[12] Qian, D., Bai, L., Wang, Y.S., Song, F., Wang, X.L. and Wang, Y.Z. A bifunctional alginate-based composite hydrogel with synergistic pollutant adsorption and photocatalytic degradation performance. *Industrial & Engineering Chemistry Research*, 58(29):13133-13144, 2019.

[13] Lei, W., Suzuki, N., Terashima, C. and Fujishima, A. Hydrogel photocatalysts for efficient energy conversion and environmental treatment. *Frontiers in Energy*, 15:577–595, 2021.

[14] Kuckhoff, T., Landfester, K., Zhang, K.A. and Ferguson, C.T. Photocatalytic hydrogels with a high transmission polymer network for pollutant remediation. *Chemistry of Materials*, 33(23):9131-9138, 2021.

[15] Katzenberg, A., Raman, A., Schnabel, N.L., Quispe, A.L., Silverman, A.I. and Modestino, M.A. Photocatalytic hydrogels for removal of organic contaminants

from aqueous solution in continuous flow reactors. *Reaction Chemistry & Engineering*, 5(2):377-386, 2020.

[16] Yang, J., Li, Z. and Zhu, H. Adsorption and photocatalytic degradation of sulfamethoxazole by a novel composite hydrogel with visible light irradiation. *Applied Catalysis B: Environmental*, 217:603-614, 2017.

[17] Sharma, G., ALOthman, Z.A., Kumar, A., Sharma, S., Ponnusamy, S.K. and Naushad, M. Fabrication and characterization of a nanocomposite hydrogel for combined photocatalytic degradation of a mixture of malachite green and fast green dye. *Nanotechnology for Environmental Engineering*, 2:1-7, 2017.

[18] Al-Aidy, H. and Amdeha, E. Green adsorbents based on polyacrylic acid-acrylamide grafted starch hydrogels: the new approach for enhanced adsorption of malachite green dye from aqueous solution. International Journal Of Environmental Analytical Chemistry, 101(15):2796-2816, 2021.

[19] Shafiee, M.R.M., Parhizkar, J. and Radfar, S. Removal of Rhodamine B by g-C_3N_4/Co_3O_4/MWCNT composite stabilized in hydrogel *via* the synergy of adsorption and photocatalysis under visible light. *Journal of Materials Science: Materials in Electronics*, 30(13), pp.12475-12486, 2019.

[20] Wei, S., Zhang, X., Zhao, K., Fu, Y., Li, Z., Lin, B. and Wei, J. Preparation, characterization, and photocatalytic degradation properties of polyacrylamide/calcium alginate/TiO_2 composite film. *Polymer Composites*, 37(4):1292-1301, 2016.

[21] Gao, Y., Gu, S., Duan, L., Wang, Y. and Gao, G. Robust and anti-fatigue hydrophobic association hydrogels assisted by titanium dioxide for photocatalytic activity. *Soft Matter*, 15(19):3897-3905, 2019.

[22] Truong, V.X. and Barner-Kowollik, C. Red-Light driven photocatalytic oxime ligation for bioorthogonal hydrogel design. *ACS Macro Letters*, 10(1):78-83, 2020.

[23] Murtezi, E., Ciftci, M. and Yagci, Y. Synthesis of clickable hydrogels and linear polymers by type II photoinitiation. *Polymer International*, 64(5):588-594, 2015.

[24] Paul, T., Das, D., Das, B.K., Sarkar, S., Maiti, S. and Chattopadhyay, K.K. $CsPbBrCl_2$/g-C_3N_4 type II heterojunction as efficient visible range photocatalyst. *Journal Of Hazardous Materials*, 380:120855, 2019.

[25] Xu, H.Y., Wu, L.C., Zhao, H., Jin, L.G. and Qi, S.Y. Synergic effect between adsorption and photocatalysis of metal-free g-C_3N_4 derived from different precursors. *PloS one*, 10(11):e0142616, 2015.

[26] Kiskan, B., Zhang, J., Wang, X., Antonietti, M. and Yagci, Y.. Mesoporous graphitic carbon nitride as a heterogeneous visible light photoinitiator for radical polymerization. *ACS Macro Letters*, 1(5):546-549, 2012.

[27] Kumru, B., Shalom, M., Antonietti, M. and Schmidt, B.V. Reinforced hydrogels *via* carbon nitride initiated polymerization. *Macromolecules*, 50(5):1862-1869, 2017.

[28] Akhundi, A. and Habibi-Yangjeh, A. Ternary g-C3N4/ZnO/AgCl nanocomposites: synergistic collaboration on visible-light-driven activity in photodegradation of an organic pollutant. *Applied Surface Science*, 358:261-269, 2015.

[29] Quan, W., Bao, J., Meng, X., Ning, Y., Cui, Y., Hu, X., Yu, S. and Tian, H. 2D/2D Z-scheme photocatalyst of g-C_3N_4 and plasmonic Bi metal deposited Bi_2WO_6: enhanced separation and migration of photoinduced charges. Journal of Alloys and Compounds, 946:169396, 2023.

[30] Tian, H., Liu, M. and Zheng, W. Constructing 2D graphitic carbon nitride nanosheets/layered MoS2/graphene ternary nanojunction with enhanced photocatalytic activity. *Applied Catalysis B: Environmental*, 225:468-476, 2018.

[31] Bao, J., Jiang, X., Huang, L., Quan, W., Zhang, C., Wang, Y., Wang, H., Zeng, Y., Zhang, W., Ma, Y. and Yu, S. Molybdenum disulfide loading on a Z-scheme graphitic carbon nitride and lanthanum nickelate heterojunction for enhanced photocatalysis: Interfacial charge transfer and mechanistic insights. *Journal of Colloid and Interface Science*, 611:684-694, 2022.

[32] Cao, Q., Barrio, J., Antonietti, M., Kumru, B., Shalom, M. and Schmidt, B.V. Photoactive graphitic carbon nitride-based gel beads as recyclable photocatalysts. *ACS Applied Polymer Materials*, 2(8):3346-3354, 2020.

[33] Kumru, B., Antonietti, M. and Schmidt, B.V. Enhanced dispersibility of graphitic carbon nitride particles in aqueous and organic media *via* a one-pot grafting approach. *Langmuir*, 33(38):9897-9906, 2017.

[34] Kumru, B., Molinari, V., Hilgart, M., Rummel, F., Schäffler, M. and Schmidt, B.V. Polymer grafted graphitic carbon nitrides as precursors for reinforced lubricant hydrogels. *Polymer Chemistry*, 10(26):3647-3656, 2019.

[35] Ye, B., Yao, C., Yan, M., Zhang, H., Xi, F., Liu, J., Li, B. and Dong, X. Photo-Induced Hydrogel Formation Based on g-C_3N_4 Nanosheets with Self-Cross-Linked 3D Framework for UV Protection Application. *Macromolecular Materials and Engineering*, 304(1):1800500, 2019.

[36] Menceloglu, Y., Menceloglu, Y.Z. and Seven, S.A. Triblock superabsorbent polymer nanocomposites with enhanced water retention capacities and rheological characteristics. *ACS omega*, 7(24):20486-20494, 2022.

[37] Zhan, Y., Liu, Z., Liu, Q., Huang, D., Wei, Y., Hu, Y., Lian, X. and Hu, C. A facile and one-pot synthesis of fluorescent graphitic carbon nitride quantum dots for bio-imaging applications. *New Journal of Chemistry*, 41(10):3930-3938, 2017.

[38] Liu, J., Zhang, T., Wang, Z., Dawson, G. and Chen, W. Simple pyrolysis of urea into graphitic carbon nitride with recyclable adsorption and photocatalytic activity. *Journal of Materials Chemistry*, 21(38):14398-14401, 2011.

[39] Çavuş, S. and Gül, G. 2-Acrylamido-2-methyl-1-propane Sulfonic Acid Based Ionic Liquid: Structural and Thermal Characterization. *Acta Physica Polonica A*, 137(4):554-556, 2020.

[40] Bao, Y., Ma, J. and Li, N. Synthesis and swelling behaviors of sodium carboxymethyl cellulose-g-poly (AA-co-AM-co-AMPS)/MMT superabsorbent hydrogel. *Carbohydrate Polymers*, 84(1):76-82, 2011.

[41] Du, W., Slaný, M., Wang, X., Chen, G. and Zhang, J. The inhibition property and mechanism of a novel low molecular weight zwitterionic copolymer for improving wellbore stability. *Polymers*, 12(3):708, 2020.

[42] Kumru, B., Molinari, V., Dünnebacke, R., Blank, K.G. and Schmidt, B.V. Extremely compressible hydrogel *via* incorporation of modified graphitic carbon nitride. *Macromolecular Rapid Communications*, 40(4):1800712, 2019.

[43] Schneider, J.T., Firak, D.S., Ribeiro, R.R. and Peralta-Zamora, P. Use of scavenger agents in heterogeneous photocatalysis: Truths, half-truths, and misinterpretations. *Physical Chemistry Chemical Physics*, 22(27):15723-15733, 2020.

[44] El-Morsi, T.M., Budakowski, W.R., Abd-El-Aziz, A.S. and Friesen, K.J. Photocatalytic degradation of 1, 10-dichlorodecane in aqueous suspensions of TiO_2: a reaction of adsorbed chlorinated alkane with surface hydroxyl radicals. *Environmental science & technology*, 34(6):1018-1022, 2000.

[45] Fónagy, O., Szabo-Bardos, E. and Horváth, O. 1,4-Benzoquinone and 1,4-hydroquinone based determination of electron and superoxide radical formed in heterogeneous photocatalytic systems. *Journal of Photochemistry and Photobiology A: Chemistry*, 407:113057, 2021.

[46] Ruan, X., Wang, L., Liang, D. and Shi, Y. Environmental Applications of 3D g-C_3N_4-Based Hydrogel with Synergistic Effect of Adsorption and Photodegradation. *Langmuir*, 39(9):3371-3379, 2023.

[47] Alharby, N.F., Almutairi, R.S. and Mohamed, N.A. Adsorption behavior of methylene blue dye by novel crosslinked O-CM-Chitosan hydrogel in aqueous solution: Kinetics, isotherm and thermodynamics. *Polymers*, 13(21):3659, 2021.

[48] Marouch, S., Benbellat, N., Duran, A. and Yilmaz, E. Nanoclay-and TiO_2 nanoparticle-modified poly (*N*-vinyl pyrrolidone) hydrogels: a multifunctional material for application in photocatalytic degradation and adsorption-based removal of organic contaminants. *ACS Omega*, 7(39):35256-35268, 2022.

[49] Rehman, T.U., Bibi, S., Khan, M., Ali, I., Shah, L.A., Khan, A. and Ateeq, M. Fabrication of stable superabsorbent hydrogels for successful removal of crystal violet from waste water. *RSC advances*, *9*(68):40051-40061, 2019.